Some Considerations for Designing a Pneumatic Micro-droplet Generator

Bao Weijie[1, 2], Wang Yiwei[1, 2], Yang Baojun[1, 2], Wang Zhihai[1, 2] and Wang Yaohong[3]

[1] Faculty of Information, Beijing University of Technology, Beijing 100124, China
[2] Key Laboratory of Optoelectronics Technology, Beijing University of Technology, Beijing 100124, China
[3] Center for Applied Mathematics, Tianjin University, Tianjin 300072, China

E-mail: wangzhihai@bjut.edu.cn

Received xxxxxx
Accepted for publication xxxxxx
Published xxxxxx

Abstract

Micro-droplet ejection is a liquid dispensing technology that has potential applications in many fields. Specifically, pneumatic ejection is actuated by a solenoid valve, which is set to "conduction" state for a brief period of time Δt. High pressure gas of P_0 enters the liquid reservoir, then releases through a venting tube, creating a oscillating pressure waveform P(t), forcing the liquid out through a tiny nozzle to form a micro-droplet. For each actuation, P(t) is acquired by a high speed pressure sensor, and the ejection state is obtained by high speed photography and image processing methods. Some issues for the design of pneumatic micro-droplet ejector are discussed. For simulation of P(t), it is proposed within an electro-acoustic analogy picture that the acoustic resistance of the venting tube is mainly due to viscous effect and may vary with time during the whole ejection process. Based on this assumption, the calculated P(t) is more consistent with the actual measurement. Experimentally, the droplet ejection process for different length of venting tube is studied. With P_0 and Δt set, by increasing the venting tube length L, both the peak value P_{MAX1} and duration of the first positive pressure period increase, and more droplets are ejected from a single actuation. By setting different P_0, P_{MAX1} for different L is tunned to an identical and appropriate value, so that single droplet is ejected due to the first positive pressure period. However, with the increase of L, the peak value of the second positive pressure period P_{MAX2} increases. There is a certain probability that another droplet is ejected. It is realized that the increase of L can reduce gas consumption, but the multiple ejection is a drawback that should be considered in the design of pneumatic ejection system.

Keywords: micro-droplet; pneumatic; electro-acoustic analogy; image processing

1. Introduction

Micro-droplet ejection technology [1], beside of being employed for inkjet printing, has found its applications in the field of biomedicine [2], printed electronics [3][4], 3D manufacturing etc. [5]. The traditional micro-droplet production methods employ thermal or piezoelectric actuation, and are popular in inkjet printing. There are a lot of progress made in non-standard micro-droplet ejection methods [6]. As an example of non-standard ejection technique, a simple setup of pneumatic ejector is shown in Fig. 1. A liquid reservoir is connected with a high-pressure gas source through a high-

speed solenoid valve, and is connected with the atmosphere through a venting tube. The high-speed solenoid valve is set to "conduction" state for a short period of time Δt, and the high-pressure gas enters the reservoir, from a gas source of pressure P_0. The gas is then released through the venting tube. A pressure pulse P(t) is generated in the reservoir, forcing the liquid out through the nozzle to form micro-droplets. The pneumatic micro-droplet generator is simple to operate, compatible with liquids of wide ranges of viscosity [7] and temperature [8]. A slightly modified pneumatic device can produce single droplet of even wider range of fluid characteristics [9]. Pneumatic droplet ejection technology is widely used in electronic packaging [10], metal 3D printing [11][12], bio-medicine etc. [13][14]. In addition, compared with piezoelectric actuation, shear stress during a pneumatic ejection is negligibly small. Initially used for cell printing, it achieved nearly 100% cell viability [15], making it a potential choice for dispensing cell laden biomedical samples.

In addition to those application research, some literatures also focused on the ejection process. Pneumatic micro-droplet ejection is a complex multi-phase flow process driven by the pressure pulse P(t), with consideration of instability caused by the surface tension effects [16]. In the pneumatic micro-droplet generator, the pressure pulse waveform P(t) is strongly related to the droplet ejection state. The process of the ejection can be simulated by solving a multi-phase flow problem, in which the volume of fluid (VOF) method is used to describe the interface [17]. Many ejection parameters, such as source pressure, actuation of the solenoid valve, geometry of the reservoir and venting tube, are relevant to the pressure pulse P(t) and therefore to the ejection process [18]. Complex alternating positive / negative P(t) has been applied to reduce the droplet size [19][20]. Simulation of P(t) can be helpful for the design of pneumatic droplet ejection system. It is pointed out that after the solenoid valve is closed, the reservoir and the venting tube form a Helmholtz resonator [18], so the oscillation of P(t) is well understood [21]. In our previous publication, a preliminary simulation model of P(t) on the basis of electro-acoustic analogy was presented [22].

There are many researches focusing on the design and optimization of the ejection system. Nozzle geometry is optimized by numerical simulation to reduce the droplet size, which was confirmed by experimental results [23]. The effects of nozzle wetting properties on droplet size and ejection process were also studied numerically and experimentally [24]. Improvement of ejection frequency and stability was realized by using a star-shaped nozzle [12][25]. Besides the nozzle, the venting tube is another component that can be easily replaced. Opening state of the venting tube drastically modify the pressure pulse P(t) [18]. For the design of pneumatic droplet ejection system, how to choose the length of the venting tube, denoted as L in the paper, is a practical issue. According to our literature survey, this topic has not been discussed thoroughly. As has been explained, the oscillating behavior of P(t) is relevant to the venting tube length. In this paper, we further optimize the electro-acoustic analogy model presented in our previous publication [22]. Here, the acoustic resistances of the venting tube and the solenoid valve are discussed in more detail. The simulation results of P(t) are consistent with the measured results. Although the source pressure P_0 (the pressure beyond the ambient pressure) is less than the ambient pressure in our experiment, some response of P(t) is not linear as P_0 is changed, which is beyond the scope of this linear model of electro-acoustic analogy. Experimentally, the influence of the venting tube length on the ejection process are studied through high-speed photography and image processing. If both P_0 and Δt are set, for longer venting tube, the first positive pressure period becomes higher in amplitude (referred as P_{MAX1}) and longer in duration, so more droplets are ejected from single actuation of the solenoid valve. For evaluating ejectors of different tube lengths, it is reasonable to, by setting different P_0, make their values of P_{MAX1} equal, so that single droplet is ejected due to the first positive pressure period. With the increase of L, the generation of the droplet is delayed. The smallest droplet is generated by using a moderate length venting tube. More importantly, with the increase of L, the amplitude of the second positive pressure period, denoted as P_{MAX2}, increases. For the longest venting tube tested in our experiment, there is certain probability that another droplet is ejected due to the second period of positive pressure. Although increasing L can reduce the gas consumption, it leads to the increase of the droplet volume and the unreliability of the ejection process. These are practical issues that need to be considered in the design of pneumatic ejection system.

2. Pneumatic micro-droplet generator and its working principles

Referring to our previous publication [22], the in-lab built pneumatic micro-droplet generator is shown in Fig. 1. The setup includes a micro-droplet ejector and an attached monitoring module. The ejector includes a liquid reservoir, a nozzle, a high-speed solenoid valve, a pressure regulator, and air path (mainly, a venting tube and a T-joint); the monitoring module includes a high speed CMOS Camera with LED illumination for visual monitoring, and a high-speed pressure sensor for monitoring the gas pressure in the reservoir. Both the ejection system and the monitoring module are operated automatically by a controller. The gas source is pure Nitrogen gas.

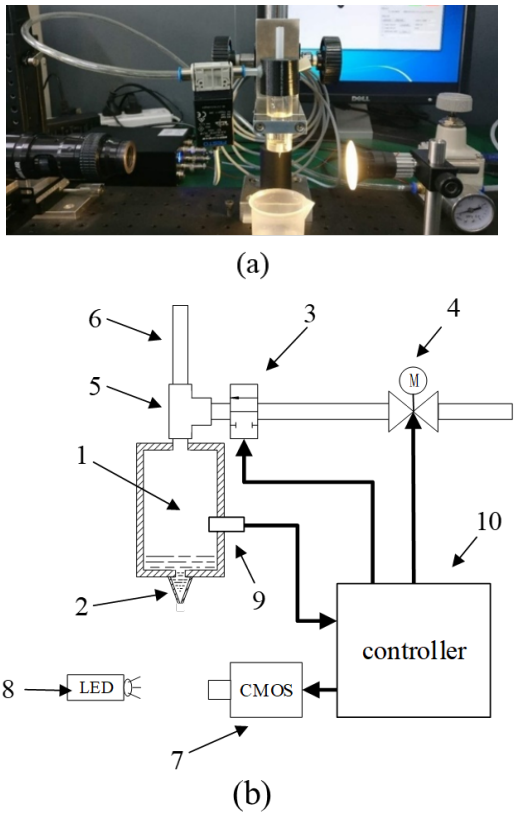

Figure 1. (a) photo of the home-build pneumatic micro-droplet generator, (b) Schematic representation of a pneumatic micro-droplet generator. It consist of a reservoir (1), a nozzle (2), a high speed solenoid valve (3), a pressure regulator (4), a T-joint (5), a venting tube (6). The micro-droplet ejection is monitored by a camera (7) with LED illumination (8). The gas pressure in the reservoir is monitored by a high speed pressure sensor (9). The micro-droplet ejection and monitoring are automatically operated by a controller (10).

2.1 Measuring Pressure Pulse Waveform P(t) in the Reservoir

As just mentioned, P(t) has the most direct influence on the ejection process. A high-speed pressure sensor (acquisition frequency 10kHz, measuring range -20kPa ~ +20kPa) is used to collect the gas pressure waveform P(t) in the reservoir. A virtual oscilloscope (sampling frequency 50kHz) simultaneously acquires the analog output signal of the pressure sensor and a synchronization signal generated by the controller. The rising edge of the synchronization signal is used as trigger for the high speed solenoid valve. The duration of the "conduction" state is set to Δt by the width of the synchronization signal. This rising edge is also referred as the t = 0 for time measurement. Starting from the rising edge of the synchronization signal, corresponding pressure waveform is recorded as P(t) (0 - 100ms). After that, the pressure is negligibly small. By smoothing, high quality pressure waveform data are obtain. P(t) waveforms for a set of venting tubes of different L are shown in Fig. 2, where P_0 = 10kPa and Δt = 1.5ms.

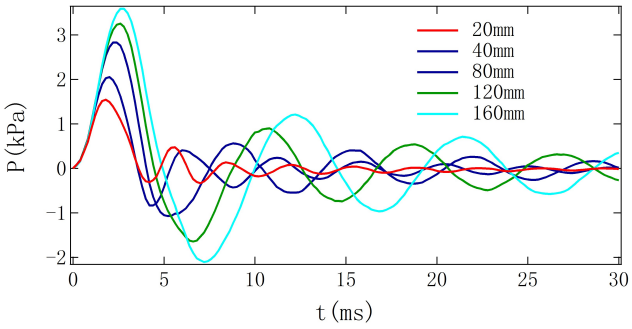

Figure 2. Pressure waveforms measured for several venting tube lengths, where source pressure P_0 = 10kPa and Δt = 1.5ms.

2.2 The Simulation of Pressure Pulse P(t) in the Reservoir

The generation of the pressure pulse in the reservoir may be understood by making an electro-acoustic analogy [26]. Specifically, the pressure in the reservoir in Fig. 3(a) and the voltage across the capacitor in the RLC circuit shown in Fig. 3(b) satisfy the same differential equation, where capacitance, inductance, and electric resistance are the electric counterparts for acoustic compliance, acoustic inertance, and acoustic resistance. The high-speed solenoid valve is equivalent to an ideal switch in series of a variable resistor, with its resistance dependent on the switching state, which will be described in detail later. The constant voltage source corresponds to the constant pressure source P_0 at the front end of the solenoid valve. In the equivalent electric circuit, when the switch is turned on, the voltage source charges the capacitor that is shunted by the inductor and the resistor. After the switch is turned off, the capacitor is discharged through the inductor and the resistor. Through a simulation (via Cadence Orcad) of the charging and discharging process, the voltage across the capacitance, or equivalently the pressure P(t) inside the reservoir is calculated.

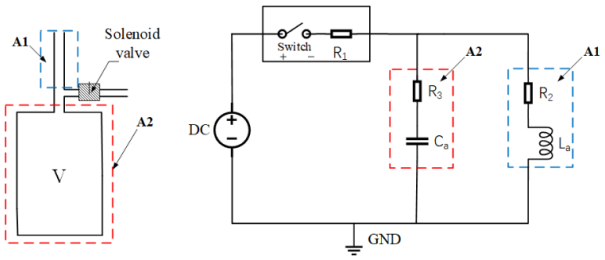

Figure 3. (a) The micro-droplet generator comprising mainly the solenoid valve, the reservoir, and the venting tube, where "V" is the volume of gas (volume above the liquid level). (b): electro-acoustic analogy, in which acoustic compliance corresponds to capacitance, acoustic inertance corresponds to inductance, acoustic resistance corresponds to electric resistance. The solenoid valve is equivalent to an ideal switch in series with a variable resistor, with a higher resistance value when the solenoid valve is turning on and shutting

off. The constant voltage source corresponds to the constant pressure P_0 at the front end of the solenoid valve.

Note that the acoustic compliance of the liquid reservoir (capacitance in the electro-acoustic analogy) and acoustic inertance of the venting pipe (inductance in the electro-acoustic analogy) can be calculated by

$$C_a = V_0/\rho_0 c^2 \quad (1)$$

$$L_a = \rho_0(L + 1.4a)/\pi a^2 \quad (2)$$

where $V_0 = 1.77\times10^{-5}\mathrm{m}^3$ is the volume of the liquid chamber (above the liquid level), L and a are length and inner radius of the venting tube. For all venting tubes in our experiment a = 1.75mm. $\rho_0 = 1.14\mathrm{kg}\cdot\mathrm{m}^{-3}$ is the density of Nitrogen gas, and c = 352m/s is speed of sound in Nitrogen gas at room temperature.

Based on our previous analysis [22], for an ejector with a fixed venting tube (specifically 80mm long), the duration of the first positive pressure period corresponds to roughly the period of time that the solenoid valve is "ON". The amplitude of the waveform is largely determined by P_0. The pressure oscillation is associated with the well-known Helmholtz cavity [21], with its resonating frequency equaling

$$\omega = c\sqrt{\pi a^2/V(L + 1.4a)} \quad (3)$$

where L, a, and c have been defined earlier. The oscillation behavior can also be understood by the LC oscillation of the equivalent electric circuit. It is worth noting that in our previous publication [22], the acoustic resistance of the venting tube and the solenoid valve was not discussed in detail. At that time, R_3 is zero, both R_1 and R_2 were set manually by trial and error, and obtained the simulation results closest to the experimentally measured results.

As the main topic of this paper is the influence of the venting tube length (20 mm-140 mm) on the pressure pulse P(t), setting the acoustic resistance of the venting tube becomes relevant. The acoustic resistance of the venting tube is composed of two parts: due to viscous force and radiation. At angular frequency ω, the viscous resistance and the radiation resistance are respectively

$$R_v = L\times\sqrt{2\eta\omega\rho_0}/\pi a^3 \quad (4)$$

$$R_r = \rho_0\omega^2/4\pi c \quad (5)$$

where viscosity coefficient $\eta = 1.8\times10^{-5}\mathrm{Pa}\cdot\mathrm{s}$ and density $\rho_0 = 1.14\mathrm{kg}/\mathrm{m}^3$ for Nitrogen gas at room temperature. L and a are defined earlier. As the Helmholtz oscillation is the most important characteristic of P(t), it may be reasonable to take $\omega = \omega_H$ in equations (4) and (5) to calculate the total acoustic resistance of the venting tube, as $R_H = R_v(\omega_H) + R_r(\omega_H)$. A simple calculation shows that the radiation damping is far less than the viscous damping, as shown in Table 1. We can ignore the radiation damping effect. The solenoid valve is equivalent to an ideal switch in series with a time-varying resistor. The acoustic resistance of the fully "ON" state is R_s, while that of the nearly "OFF" state is R_s'. The value of R_s affects the amplitude of P(t). Setting appropriate R_s' makes the rising edge of P(t) close to the experimental results. Since we do not know the internal structure of the solenoid valve, the value of R_s and R_s' are set manually by trial and error, to get the best simulation results.

As a self-consistency check, the pressure waveform P(t) after the shut-off of the solenoid valve is examined. The Helmholtz resonator is equivalent to the well-known RLC electric circuit. As the system is in the under-damped region, the amplitude decays exponentially, $P_A \propto \exp(-\alpha t)$, where $\alpha = R/2L_a$ is the attenuation coefficient. Figure 4 shows the amplitude versus time, and the values of α for different venting tube lengths are obtained via curve fitting. From the acoustic inertance L_a, it is shown that the acoustic resistance $2\alpha L_a$ is slightly larger than R_H calculated by equations (4) and (5), as summarized in Table 1. This additional acoustic resistance ranges $0.25 - 0.45\times10^6$ ($\mathrm{kg}\cdot\mathrm{m}^{-4}\mathrm{s}^{-1}$), and is not significantly dependent on the venting tube length. We speculate that it may be due to some damping effect in the reservoir, which is represented by R_3 in Fig. 3.

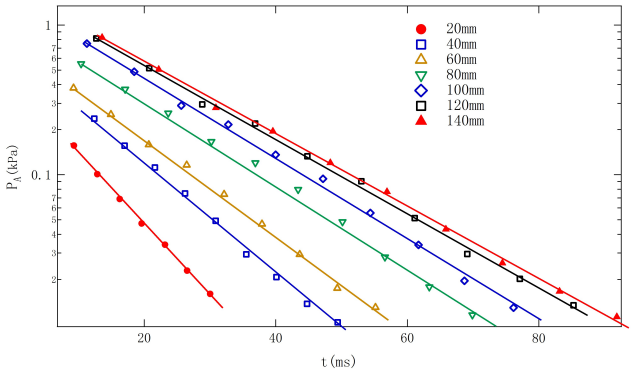

Figure 4. Amplitude of P(t) versus time in log scale, for several venting tube lengths.

For a set of venting tube lengths, the calculated values of acoustic compliance, inertance, and resistances are shown in Table 1. Cadence OrCAD is used to simulate the equivalent electric circuit. In our initial attempt, we simply set $R_2 = R_H$. However, such a model gets into difficulties. As an example, for L = 80mm, as shown in Fig. 5(a), with $R_2 = R_H$, the amplitude of the first negative period is even significantly greater than P_{MAX1}, which is contradictory to the experimental results, shown in Fig. 2. This difficulty may be alleviated by setting R_2 (5.5×10^6, to be specific) much larger than the R_H. Unfortunately, in this case, the oscillation amplitude will decay rapidly, shown in Fig. 5(b). In the experiment, however, after the solenoid valve is closed, the pressure oscillation decays slowly and can last up to 10 cycles.

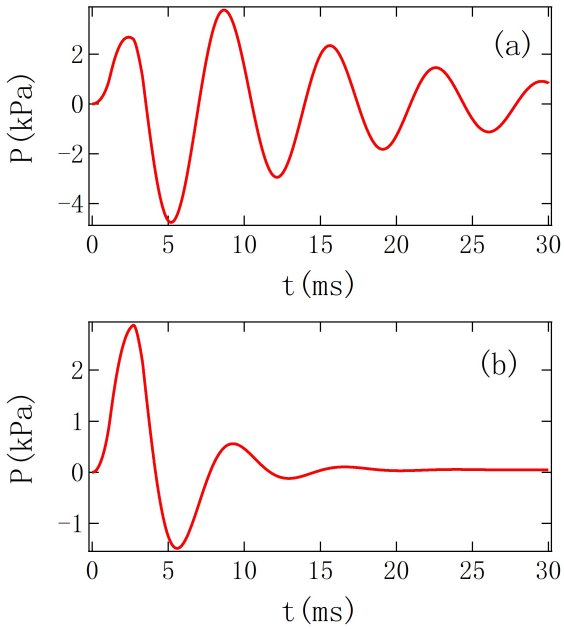

Figure 5. (a) Simulated P(t) with R_2 calculated via equations (4) and (5). (b) Simulated P(t) with $R_2 = 5.5\times10^6$, which is significantly larger than R_H obtain from equation (4) and (5) for Helmholtz frequency.

tube length /mm	20	40	60	80	100	120	140	160
C_a	1.25×10^{-10}							
L_a	2.66	5.03	7.40	9.77	12.15	14.52	16.89	19.26
ω_H	1732	1260	1038	904	811	741	688	644
R_v	0.32	0.54	0.74	0.92	1.08	1.24	1.40	1.55
R_r	0.01	0.006	0.004	0.003	0.003	0.002	0.002	0.002
$2\alpha L_a$	0.59	0.88	1.08	1.27	1.51	1.65	1.86	1.93
R_a	3.3	4.2	5	5.5	5.9	6.1	6.5	6.4
R_s	20							
R'_s	60							

Table 1. Values of acoustic compliance, inertance, and resistances, where C_a is the acoustic compliance associated with the reservoir, L_a is the acoustic inertance of the venting tube. ω_H is the angular frequency of the Helmholtz oscillation. R_v and R_r are acoustic resistances at ω_H due to the viscosity and radiation respectively, R_s and R'_s are respective acoustic resistances for fully open and nearly closed solenoid valve. R_a represents the amplitude of R_2 and is defined in Fig. 6(a). $2\alpha L_a$ is an effective acoustic resistance, where attenuation coefficient α can be estimated from the damping behavior of P(t), see Fig. 4. The respective units for acoustic compliance, inertance, and resistance are $s^2m^4 \cdot kg^{-1}$, $10^3kg \cdot m^{-4}$, and $10^6kg \cdot m^{-4}s^{-1}$

To solve those problems, we propose a modified model. Although a quantitative formula is not given here, the viscous resistance R_2 of the venting tube may be greater than R_H during the actuation of the solenoid valve. Considering that the turn-on and shut-off times of the solenoid valve, referred as t_{ON} and t_{OFF}, are 1.2ms and 0.6ms respectively, while Δt is 1.5ms, all these characteristic times are far less than the period of Helmholtz oscillation ($T_H = 2\pi/\omega$). Therefore, frequency components associated with the actuation of the solenoid valve are much higher than the Helmholtz frequencies. The schematic representation of acoustic resistance versus time is shown in Fig. 6(a). After the valve is completely opened or closed, R_2 will drops back to R_H over 1/2 of T_H. The choice of 1/2 seems to give more reasonable simulation results. During the opening of the valve, $R_2 = R_a$. Please note that t_{OFF} is half of t_{ON}. This leads to higher frequency components, and enhanced resistance ($R_2 = \sqrt{2}R_a \approx 1.4R_a$, shown in Fig. 6(a)) during the shut-off. The principle for setting R_a is to make the simulated P(t) closest to the experimental results. The finally accepted values of R_a are shown in Table 1. In Cadence OrCAD, simulation of such time-varying resistance can be realized by a RVAR function [27]. In this modified model, pressure pulse P(t) for several different lengths of venting tubes are simulated. The consistency between the experimental result (Fig. 2) and simulation (Fig. 6(b)) is obviously improved. Within this picture, the acoustic resistance of the solenoid valve is taken to be independent of the venting tube, as it is mainly determined by those characteristic time scales (t_{ON}, t_{OFF}, and Δt) and the internal structure of the solenoid valve.

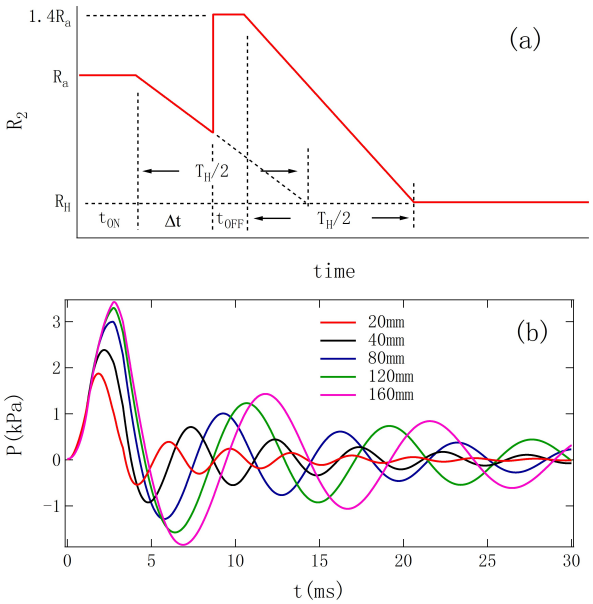

Figure 6. (a) Schematic representation of R_2 versus time. (b) Simulated P(t) for several venting tube lengths, with R_2 shown in panel (a), P_0=10kPa, Δt=1.5ms.

Although the simulation results are in good agreement with the measured pressure waveforms, this model is still not satisfactory. The much stronger transient acoustic resistance proposed in this model is associated with that higher frequency components are produced by the quicker solenoid valve actuation. However, R_a is far from being proportional to

the length of the venting tube. Therefore, the proposed picture is not self-consistent. Besides, the electro-acoustic analogy model is only appropriate for the case where P_0 is far less than 1 atm. For a set of higher P_0, P(t) is experimentally measured. For ejector with L = 20mm venting tube, as shown in Fig. 7(a), the amplitude of the first positive pressure period P_{MAX1} is not strictly proportional to P_0. What is more confusing is that on increasing P_0, the second maximum (as indicated by the arrow in Fig. 7(a)) P_{MAX2} decreases in amplitude, and shifts to earlier moment t_{MAX2}. For P_0 = 50kPa and 60kPa, the second maximum has become the right shoulder of the first positive pressure period. Those effects certainly cannot be explained by this linear model of electro-acoustic analogy. For a sufficiently long venting tube, L = 140mm, P_{MAX1} is still not proportional to P_0. Unlike the case of short venting tube, P_{MAX2} increases monotonically with P_0, and change of t_{MAX2} is less significant. Note that here an even shorter Δt = 1ms is used, the non-linear behaviors shown in Fig. 7(a) are also observed for longer Δt=1.5ms, although slightly less prominent.

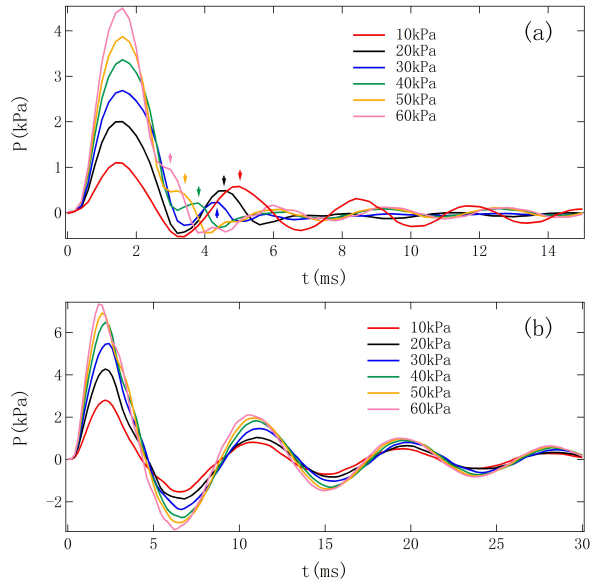

Figure 7. Experimentally measured P(t) for several P_0 for two different venting tubes, (a) L = 20mm, (b) L = 140mm. The solenoid valve is "ON" for Δt = 1.0ms for both panels

2.3 Machine-vision Based Ejection State Monitoring

The photography system is mainly composed of a high-brightness LED and a high-speed CMOS camera (Model mini AX100 from Photron). The purpose of the system is to monitor the process of micro-droplet ejection. Photographing is done by using a back-lightening configuration, with the nozzle staying between the LED and the camera. The frame rate is set to be 15000 fps, and the exposure time is set to be 50μs.

The methods of image processing may be found in our previous publication [22]. Briefly, a region of interest (ROI) of the original image is specified first to improve image processing efficiency. This is because the nozzle and droplet only occupy a small region of the whole image. In the second step, binarization of the ROI is performed by utilizing an automatic threshold segmentation method (Otsu algorithm) for grayscale images. Due to refraction effect, there is tiny bright region within the droplet. For not to affect the subsequent extraction of the droplet information, in the 3rd step, an image filling algorithm may be used to have the bright region removed. The complete droplet area is then labeled by a connected region analysis. On this basis, the number of droplets, and the geometrical parameters of each droplet are obtained. Especially, for the droplet volume, from the image of the droplet, the waist of the droplet w is measured versus vertical coordinate z, both in numbers of pixels. The droplet volume is calculated via $V = \sum_z \pi[w(z)/2]^2$. Then, it is converted to volume in nanoliter, based on the magnification of the imaging system.

3. Experimental studies on droplet ejection systems with different venting tube lengths

The ejection experiment is performed with DI water, using a 300μm internal diameter nozzle (Musashi engineering), with ejection frequency set to 10 Hz. The source pressure P_0 at the front end of the solenoid valve is tuned by a pressure regulator (SMC Corporation) in the range of 5 - 60 kPa. The change of liquid level is negligible during the experiment, so the volume V left for the gas is fixed.

3.1 Same P_0 and Δt, different venting tube lengths

First of all, fixing the source pressure P_0 = 10 kPa, the duration of the "conduction" state is set to Δt = 1.5ms, a set of pressure waveforms P(t) are obtained by changing the length of the venting tube. Some of those are shown in Fig. 2. With the increase of L, both the amplitude and duration of the first positive pressure cycle increase, so more droplets are produced, as summarized in Table 2.

tube length /mm	20	40	60	80	100	120	140	160
P_{MAX1} /kPa	1.5	2.1	2.6	2.8	3.0	3.25	3.4	3.55
number of droplets	0	0	1	Mostly 1	1-2	Mostly 2	2-4	3-5

Table 2. Peak value of the first positive pressure period (P_{MAX1}) and the number of droplets, for a set of venting tube lengths, P_0 = 10kPa, Δt = 1.5ms.

3.2 Same P_{MAX1} and Δt, different venting tube lengths

Usually, each time the solenoid valve is actuated, ejection of single droplet is expected. The number of droplets highly depends on the amplitude of the first positive pressure period. Therefore, for evaluating a set of venting tubes of different lengths, keeping P_{MAX1} identical is a reasonable choice, as

shown in Fig. 8. This is done by setting different source pressure P_0 for different tube length, as summarized in Table 3. The selection of P_{MAX1} is based on the following principle: a droplet can be stably ejected due to the first positive pressure period. Here, the L = 160mm tube is not used, simply because the P_0 needed is too low for our pressure regulator. As summarized in Table 3, the throughput of the venting tube per actuation is estimated by integrating the volume velocity (the current flowing through L_a and R_2 in the equivalent circuit).

tube length /mm	20	40	60	80	100	120	140
breakup time /ms	5.2	5.3	5.1	5.5	5.5	5.8	6.3
droplet volume /nL	187	158	150	145	140	144	182
source pressure P_0 /kPa	17	11.5	9.7	8.6	7.7	7	6.3
throughput of venting tube /mL	2.0	1.32	1.1	0.98	0.9	0.83	0.75

Table 3. The breakup time t_B and the droplet volume generated by ejectors of different venting tube lengths. P_{MAX1} = 2.5kPa, Δt = 1.5ms. The required source pressure P_0 and estimated throughput of the venting tube.

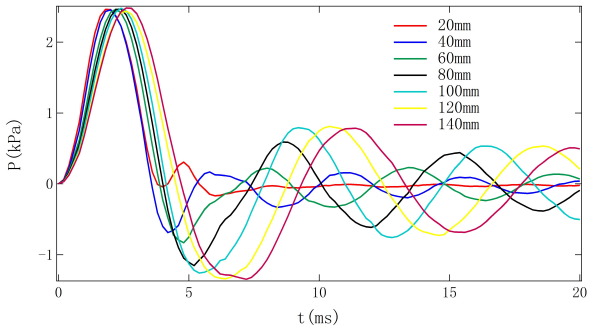

Figure 8. Pressure pulses P(t) in the reservoir taken for several venting tube lengths. Here, P_0 is set so that P_{MAX1} are identical for all those pulses.

By using the high-speed camera, the breakup time can be accurately measured. Table 2 shows the breakup time of droplet for several venting tube lengths. With the increase of L, t_B tends to increase. We speculate that the delay of breakup is due to the increase of duration of the first positive pressure period. It has been proposed that negative pressure contributes to the breakup of the liquid and the formation of droplets [18]. This is consistent with our experimental results. Also shown in Table 2, on increasing L, the droplet volume slightly decreases, reaches minimum at L = 100mm, then slightly increases. It is worth mentioning that the most effective way to reduce the volume is still to reduce the inner diameter of the nozzle. For the current system, with a nozzle of 100μm inner diameter, droplet volume can be as small as 6.3nL.

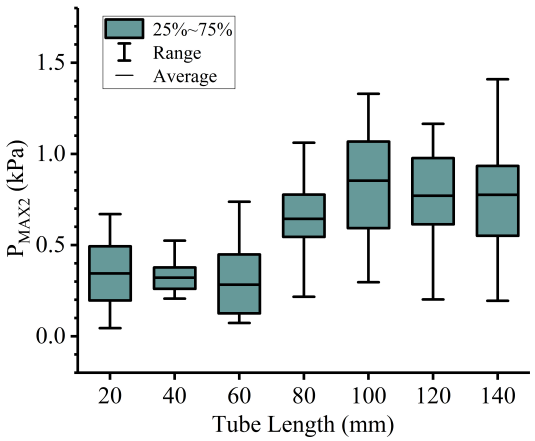

Figure 9. Variation of P_{MAX2}, from 20 measurements, for several venting tube lengths. The box includes 50% of the total events.

More importantly, as can be seen from Fig. 8, with the increase of the venting tube length, peak value of the second positive pressure period P_{MAX2} increases significantly, and saturates for sufficiently long venting tube. It should be mentioned that each curve in Fig. 8 is the average of 20 measurements. Although not shown here, the fluctuation of t_{MAX1}, defined via $P(t_{MAX1})=P_{MAX1}$, is almost negligible, while that of t_{MAX2}, defined via $P(t_{MAX2})=P_{MAX2}$, is ±0.2-0.3ms. The fluctuation of P_{MAX1} is only 0.08kPa, while that of P_{MAX2} can be as large as ±0.2-0.6kPa, summarized in Fig. 9 for several venting tube lengths. Although the averaging will smooth out some occasional disturbances and lower the amplitude of the pressure oscillation to a some extent, the averaged P(t) still rather well reflects the shape of individual pressure pulse. We speculate that although Δt is set to 1.5ms, the actual duration of the "conduction" state t_C fluctuates. This fluctuation of t_C may significantly deteriorates the consistency of P_{MAX2} and t_{MAX2}. Shortly, we will point out that the fluctuation of P_{MAX2} will have adverse effects on ejection stability. It is straightforward that any change of t_C leads to shift of t_{MAX2}. However, the cause of P_{MAX2} fluctuation is not clear at present, simply because pressure pulses with larger P_{MAX2} do not necessarily have larger t_{MAX2}.

Figure 10(a) shows the ejection process for an ejector, with L = 80mm, Δt = 1.5ms, and P_0 is tuned at 8.6kPa to make P_{MAX1} = 2.5kPa. For each actuation of the solenoid valve, single droplet is generated, with rather good stability and consistency. Typical pressure pulse is shown in black in Fig. 10(c).

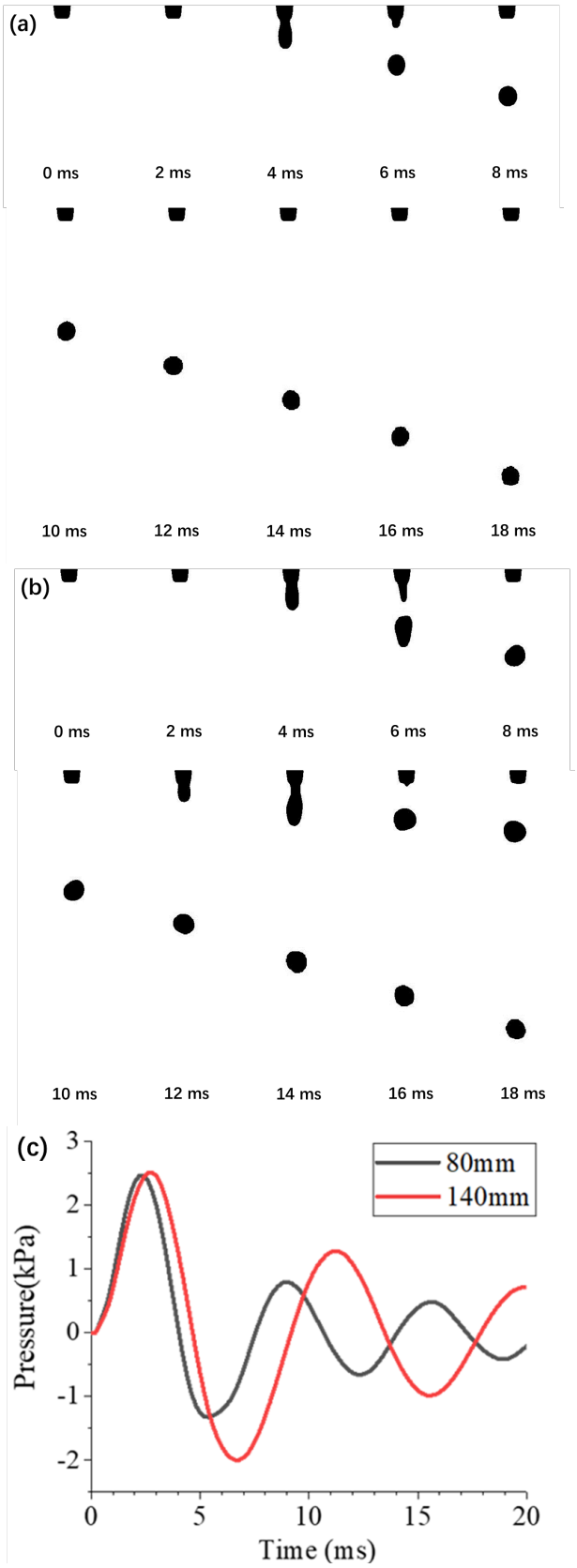

Figure 10. Ejection process for ejectors with (a) 80mm and (b) 140mm long venting tubes. The pressure pulses are shown in (c), where P_{MAX1} is set to 2.5kPa for both.

In a similar experiment, an ejector with L = 140mm venting tube is tested, where Δt is set to 1.5ms, and a lower P_0 =6.3kPa is applied to keep P_{MAX1} = 2.5kPa (see table 3). Consistently, one droplet is generated, due to the first period of positive pressure. However, another droplet is likely ejected, due to the second positive pressure period, shown in Fig. 10(b). Ejection of two droplets per actuation accounts for 15% of the total cases, 3 from 20 actuations in our experiment. For all 20 actuations, although with Δt set to 1.5ms, P_{MAX2} exhibits clear fluctuation, likely due to fluctuation of t_C. For the 3 cases mentioned above, P_{MAX2} ranges from 1.25 to 1.4kPa, higher than the average value of P_{MAX2} at 0.8kPa (see Fig. 9). An example of those 3 pressure waveforms, which corresponds to the ejection process in Fig. 10(b), is shown as red line in Fig. 10(c). It should be noted that a separated positive pressure period with the amplitude of 1.3kPa is certainly not enough to produce a droplet. In addition, as can be seen in Fig. 9, for L = 100mm and 120mm, there are pulses with similar P_{MAX2}, but no second droplet is produced. Therefore, we speculate that resonance effect between the driving pulse P(t) and the liquid movement also plays a role in the generation of the second droplet.

The highest ejection frequency f_{MAX} at which the system can function properly have been examined for several vent tube lengths. With the 20mm venting tube, the highest ejection frequency can reach 70Hz. For L = 60mm, f_{MAX} is 30 - 40Hz. For L = 100mm, f_{MAX} is about 30Hz. For L = 120mm, f_{MAX} reduces to 20Hz. With the increase of L, the decreasing trend of f_{MAX} is significant. Interplay of two factors would be the cause of this behavior. First of all, with the increase of L, as shown in Fig. 8, the period of pressure oscillation increases and the amplitude attenuation slows down. It takes longer for the liquid meniscus at the nozzle to return to equilibrium, which is confirmed by the high-speed photography. Secondly, the inconsistency of pressure waveform (mainly due to the fluctuation of t_C) makes the meniscus at the nozzle inconsistent each time the actuation is applied.

An estimate of fluctuation of t_C would be helpful for the operation of the ejection system. Any change of t_C would also lead to shift of t_{MIN1} (the time when pressure reaches its first minimum). In a measurement where the reservoir is removed and the pressure sensor is placed at the lower port of the T joint (see Fig. 1), the fluctuation of t_{MIN1} is measured for a set of venting tube lengths. For Δt set to 1.5ms, the fluctuation of t_{MIN1} is ±0.3ms. As mentioned earlier, the fluctuation of t_{MAX2} is also ±0.2-0.3ms, consistent with the current results. The fluctuation is not sensitive to the venting tube lengths, which is quite reasonable. Therefore, it is convinced that the fluctuation of t_C is ±0.3ms.

4. Conclusions

Some practical issues in the design of pneumatic micro-droplet ejector are discussed. Firstly, based on an electro-

acoustic analogy model, it is proposed that the acoustic resistance of the venting tube may vary with time during the whole ejection process. Based on this assumption, the simulated P(t) is more consistent with the actual measurement results. The droplet ejection process for different length of venting tube is studied. When both P_0 and Δt are set, on increasing L, both the peak value P_{MAX1} and the duration of the first positive pressure period increase, leading to more droplets from each actuation of the solenoid valve. The more reasonable method in parameter selection is setting different P_0 for different venting tube to make the value of P_{MAX1} consistent, single droplet can be ejected due to the first positive pressure period. With L increased, the breakup of the droplet is slightly delayed. On increasing L, the droplet volume decreases, reaches minimum for an intermediate L, and then increases. More importantly, with the increase of L, the peak value of the second positive pressure period P_{MAX2} increases. For some sufficiently long venting tube, there is a certain probability that another droplet is ejected due to the second positive pressure period. The highest allowed ejection frequency also decreases on increasing L.

For those who want to get droplet as small as possible from a particular nozzle, it is feasible to optimize the length of the venting tube. However, the effect of size reduction is not significant. If the droplet size is not a concern, the gas consumption is lower for longer venting tube. However, inconsistency of the ejection state caused by the excessive increase of the venting tube length is an issue to be considered in the design of pneumatic droplet ejection system.

References

[1] Zapka W 2018 Handbook of Industrial Inkjet Printing: A Full System Approach

[2] Gudapati H, Dey M and Ozbolat I 2016 *Biomaterials* **102** 20-42

[3] Cui Z 2016 Printed Electronics: Materials, Technologies and Applications

[4] Raut N C and Al-Shamery K 2018 **6(7)** 1618-1641

[5] Vaezi M, Seitz H, and Yang S 2013 *The International Journal of Advanced Manufacturing Technology* **67(5-8)** 1721–1754

[6] Basaran O A, Gao H and Bhat P P 2013 *Annual Review of Fluid Mechanics* **45** 85-113

[7] Banitabaei S A and Amirfazli A 2016 *Colloids and Surfaces A: Physicochemical and Engineering Aspects* **505** 204–213

[8] Moqadam S I, Madler L and Ellendt N 2019 *Micromachines* **10(7)** 477

[9] Choi I H, Kim Y K, Lee S, Lee S H and Kim J 2015 *Journal of Microelectromechanical Systems* **24(4)** 768-770

[10] Luo J, Qi L, Zhong S, Zhou J and Li H 2012 *Journal of Materials Processing Technology* **212(10)** 2066-2073

[11] Cao W and Miyamoto Y 2006 *Journal of Materials Processing Technology* **173(2)** 209-212

[12] Lass N, Riegger L, Zengerle R and Koltay P 2013 *Micromachines* **4(1)** 49-66

[13] Choi I H, Kim H, Lee S, Baek S and Kim J 2015 *Biomicrofluidics* **9(6)** 064102

[14] Chen Z, Zhang X, Chen P, Li W, Zhou K, Shi L, Liu K and Liu C 2017 *International Journal of Precision Engineering and Manufacturing* **18(5)** 755-761

[15] Wang M, Wang C, Wang F, Wang Z H, Chen X and Gui J G 2018 *Proceedings of 8th International Conference on Biomedical Engineering and Technology* 89-95

[16] Eggers J and Villermaux E 2008 *Reports on progress in physics* **71(3)** 036601

[17] Luo J, Q L i, Zhou J, Hou X and Li H 2012 *Journal of Materials Processing Technology* **212** 718-726

[18] Cheng S and Chandra S 2003 *Experiments in fluids* **34(6)** 755-62

[19] Goghari A A and Chandra S 2008 *Experiments in Fluids* **44(1)** 105-114

[20] Amirzadeh A and Chandra S *Experimental thermal and fluid science* **34(8)** 1488-1497

[21] Harris C M 1991 Handbook of acoustical measurements and noise control

[22] Wang F, Wang Y W, Bao W J, Zhang H, Li J and Wang Z H 2020 International Journal of Precision Engineering and Manufacturing **21** 633–640

[23] Zhong S Y, Qi L H, Xiong W, Luo J and Xu Q X 2017 *The International Journal of Advanced Manufacturing Technology* **93(5-8)** 1771-1780

[24] Zuo H S, Li H J, Qi L H, Luo J, Zhong S Y and Li H P 2014 *Journal of Materials Processing Technology* **214(11)** 2566-75

[25] Tropmann A, Lass N, Paust N, Metz T, Ziegler C, Zengerle R and Koltay P 2012 *Microfluidics and nanofluidics* **12(1-4)** 75-84

[26] Kinsler L E and Frey A R, Coppens A B and Sanders J V 1999 Fundamentals of acoustics

[27] Fitzpatrick D 2017 Analog design and simulation using OrCAD Capture and PSpice